HRXRD study of ZnO single crystals bombarded with Ar ions

Marek Wójcik, Jarosław Gaca, Piotr Caban, Andrzej Turos
Institute of Electronic Materials Technology
133 Wólczynska Str., 01-919 Warsaw, Poland
e-mail: Marek.Wojcik@itme.edu.pl

Abstract: High resolution X-ray diffraction methods (HRXRD) were used to study the tetragonalization of a unit cell in a zinc oxide single crystal resulting from the Ar-ion bombardment. Bulk ZnO (00·1) single crystals were bombarded with ions with the energy of 300 keV and a dose range between 1 x 10^{14} cm^{-2} and 4 x 10^{16} cm^{-2}. Diffraction profiles, obtained by radial 2Theta/Omega scans in the vicinity of the 00·4 ZnO reciprocal space node were measured and fitted to the curves calculated by means of a computer program based on the Darwin's dynamical theory of X-ray diffraction. On the basis of these numerical simulations, the profile of the interplanar spacing between planes perpendicular to the c axis of the ZnO single crystal were determined as a function of the Ar ion dose. It was found that positive deformation parallel to the c-axis appeared for the low doses in the bombarded crystal volume. When the dose is increased this deformation gets pronounced, and after reaching a certain critical value, it becomes saturated. This observation leads to the conclusion that the plastic deformation appears in the implanted volume of the crystal.

Key words: HRXRD, ZnO monocrystal, ion implantation, radiation defect analysis

Badanie metodami wysokorozdzielczej dyfraktometrii rentgenowskiej monokryształów ZnO bombardowanych jonami Ar

Streszczenie: Za pomocą wysokorozdzielczej dyfraktometrii rentgenowskiej (HRXRD) badano tetragonalizację komórki elementarnej monokryształu tlenku cynku powstałą pod wpływem bombardowania jonami Ar. Objętościowe monokryształy ZnO o orientacji (00·1) były bombardowane jonami o energii 300 keV, w przedziale dawek od 1 x 10^{14} cm^{-2} do 4 x 10^{16} cm^{-2}. Zarejestrowano profile dyfrakcyjne otrzymane metodą radialnego skanowania 2Teta/Omega, w otoczeniu węzła 00·4, sieci odwrotnej ZnO i w oparciu o założenia dynamicznej teorii dyfrakcji promieniowania rentgenowskiego w ujęciu Darwina, wykonano ich symulacje numeryczne. Na tej podstawie określono, w zależności od dawki, profil zmiany odległości płaszczyzn prostopadłych do osi c monokryształu ZnO. Stwierdzono, że dla niskich dawek, w ściśle określonej objętości kryształu, powstaje dodatnie odkształcenie równoległe do osi c, wraz ze wzrostem dawki jonów to odkształcenie wzrasta, a po osiągnięciu pewnej krytycznej wartości ulega nasyceniu. To prowadzi do wniosku, że w implantowanej objętości kryształu powstaje wówczas odkształcenie plastyczne.

Słowa kluczowe: wysokorozdzielcza dyfrakcja rentgenowska, monokryształ ZnO, implantacja jonów, analiza defektów radiacyjnych

1. Introduction

ZnO is a wide bandgap energy (Eg = 3.37eV) semiconductor. Its most important properties include direct and very high exciton binding energy (60 meV), strong piezoelectric effect, high conductivity, high heat capacity and low thermal expansion coefficient. Due to its wide potential application spectrum in microelectronics, biosensors, spintronics and light sources, ZnO has been the most intensively explored semiconductor material of the last decade [1]. Ion bombardment represents an attractive tool for semiconductor compound processing (doping, isolation etc.). However, a major drawback of this technique is the buildup of lattice disorder due to the ballistic character of this process [2, 4]. Means that in spite of the vast amount of accumulated data, the mechanism of defect buildup in ZnO is not completely elucidated.

Damage accumulation in ion-bombarded compound semiconductors is a consequence of collision damage sequential evolution in extended defects such as dislocations or stacking faults. Our study of GaN [5 - 6] revealed that damage accumulation is a three-step process. The HRXRD analysis indicated that ion bombardment to low doses causes an increase in the c parameter, thus leading to a strain buildup in the implanted region. Once the critical value of the shear stress is reached, plastic deformation due to the dislocation slip appears to take place, and as a result a dislocation tangle is formed. The transition to Stage III – amorphization – takes place at a high impurity concentration and is apparently due to the defect–impurity interaction.

2. Experimental

High-quality commercial [00·1] single ZnO crystals delivered by MaTecK, Germany, were ion-bombarded at the Institute of Electronic Materials Technology (ITME) using the Balzers MBP 202RP ion implanter with 300 keV Ar^+ ions to doses ranging from 1 x 10^{14} cm^{-2} to 1 x 10^{16} cm^{-2} at room temperature (RT). The structural characteristics of implanted ZnO monocrystals can be determined using

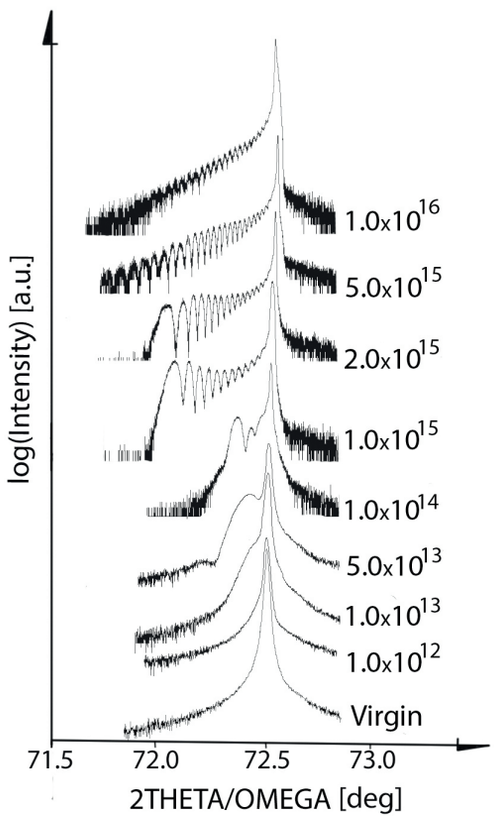

Fig. 1. X-ray diffraction profiles performing 2THETA/OMEGA scans for the virgin ZnO monocrystal implanted with doses ranging from 1 x 10^{12} cm^{-2} to 1 x 10^{16} cm^{-2}.
Rys. 1. Rentgenowskie profile dyfrakcyjne otrzymane metodą skanowania 2THETA/OMEGA dla monokryształu ZnO nieimplantowaego, a także implantowanego dawkami od 1 x 10^{12} cm^{-2} do 1 x 10^{16} cm^{-2}.

the non-destructive HRXRD method. To this end, the SmartLab diffractometer equipped with a 9 kW rotating Cu anode (wavelength $CuK_{\alpha 1}$ equals 0.15405 nm) was used to perform the X-ray diffraction measurements. The radial 2Theta/Omega diffraction profiles were recorded for the following incident optics settings: cross beam optics CBO unit, Ge(220) x 2 monochromator, open soller slit, and on the receiving side: an open soller slit and soller slit of 5.0 deg. All measured samples were adjusted in such a way that the c-axis was parallel to the φ - axis of the goniometer. So as to obtain radial scans of the (00·4) reciprocal lattice spot of the ZnO monocrystals. The resultant diffraction profiles are presented in Fig. 1.

The influence of implantation on the X-ray diffraction profile is strongly dependent on the ion dose. The shape of the 2Theta/Omega diffraction patterns in the vicinity of the 00·4 reciprocal lattice spot of the implanted ZnO monocrystal, is characterized mainly by the asymmetry that appears on the low-angle side of the afore mentioned node. This asymmetry becomes greater when the dose of Ar ions becomes increased. A relatively high and well-separated peak appears for doses ranging from 1 x 10^{14} cm^{-2} to 2 x 10^{15} cm^{-2}, on the low-angle side of the 00·4 node while for the highest doses (e.g. 5 x 10^{15} cm^{-2} and 1 x 10^{16} cm^{-2}) only some oscillations can be observed.

In order to study lattice deformation resulting from ion implantation, the collected experimental data were analyzed by means of computer simulations. The code, based on Darwin's dynamical theory of X-ray diffraction [7 - 8], was developed to perform X-ray diffraction profile simulation. For the purpose of such simulation, a heterostructure is modeled as a stack of parallel atomic planes. For each plane different chemical composition is assumed, which allows modeling graded hetero-interfaces. Based on the assumed chemical composition of the atomic planes, the code calculates the interplanar spacing between succeeding atomic planes and their scattering power. The diffraction profile for a crystal after ion irradiation can be calculated by displacing some of the atoms from their equilibrium positions in the atomic planes, and especially out of their position on the Bragg planes. This results in the modification of the interplanar atomic spacing and planar scattering power profiles [9]. The analysis is performed with the aim to diversify the chemical composition of each atomic plane (or planar scattering power and interplanar spacing) until the best fit between experimental and simulated X-ray diffraction profiles is achieved. The code was tested while working with $Al_xGa_{(1-x)}As$/GaAs superlattices to be applied as a Bragg mirror [10].

For the purpose of the simulation, the region of the ZnO monocrystal with the strain induced by ion irradiation was modeled as a stack of parallel layers, perpendicular to the c axis, each of which was 9 nm thick and differed in terms of interplanar spacing and/or planar scattering power. The profile of the interplanar spacing modulation in the growth direction was assumed to reproduce the shape of displaced atom distribution in ion-implanted ZnO [11 - 12]. This distribution was treated as the primary piece of data in X-ray profile calculations, and can be approximated by the Gaussian in the following form:

$$d(\mathrm{x}) = d_0\left(1 + \mu \exp\left(\frac{-4\ln 2(x - x_0)^2}{\sigma^2}\right)\right), \qquad (1)$$

where:
d(x) is the interplanar spacing between the (00·4) planes in the strained layer, located at an x distance from the surface, d_0 is the (00·4) interplanar spacing in virgin ZnO, μ is the maximal lattice misfit between the strained layer and virgin ZnO, x_0 is the position of the center of the Gaussian peak, and σ is the full width in the half maximum of the standard distribution.

The fit between the experimental and calculated diffraction profiles was obtained by changing the values of the x_0, σ and μ parameters (Fig. 2).

The examples of the best fits between the experimental and calculated diffraction profiles as well as strain profiles are shown in Fig. 3 - 7.

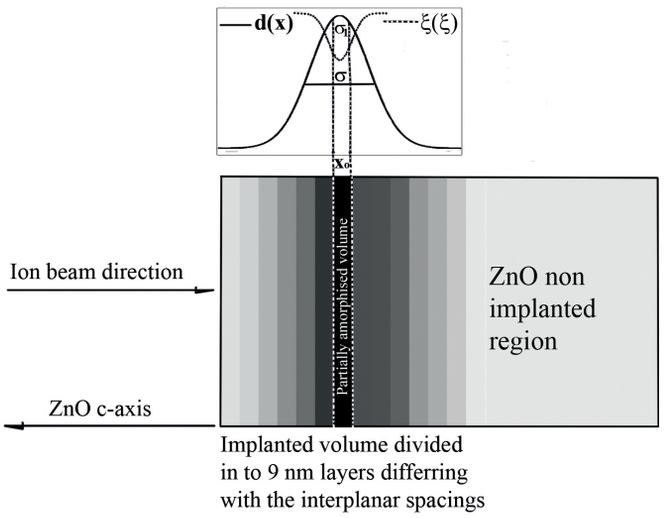

Fig. 2. Graded layer model of the strain distribution in the implanted region of the ZnO monocrystal.
Rys. 2. Model rozkładu naprężeń w implantowanej objętości monokryształu ZnO.

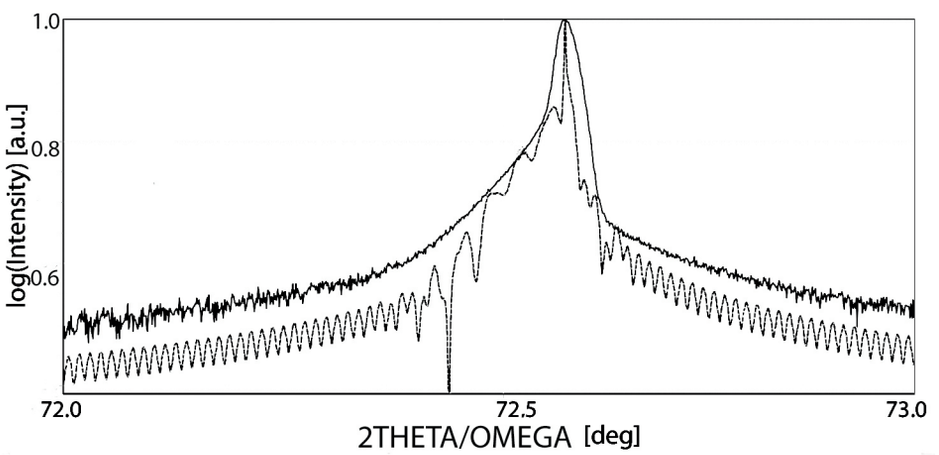

Fig. 3. X-ray diffraction profiles: experimental (solid) and calculated (dash) for the ZnO monocrystal implanted with the ion dose of 1 x 10^{13} cm^{-2}. Reflection 00·4, x_0 = 180 nm, σ = 30 nm, $\langle d \rangle$ = 0,1301666 nm, μ = 0.015365.
Rys. 3. Rentgenowskie profile dyfrakcyjne: doświadczalny (ciągły) i obliczony (przerywany) dla monokryształu ZnO implantowanego dawką 1 x 10^{13} cm^{-2}. Refleks 00·4, x_0 = 180 nm, σ = 30 nm, $\langle d \rangle$ = 0,1301666 nm, μ = 0,015365.

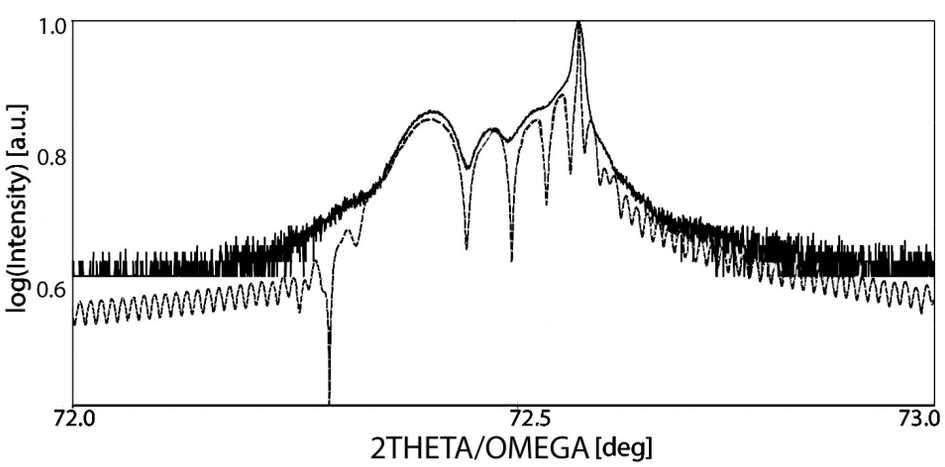

Fig. 4. X-ray diffraction profiles: experimental (solid) and calculated (dash) for the ZnO monocrystal implanted with the ion dose of 1 x 10^{14} cm^{-2}. Reflection 00·4, x_0=180 nm, σ = 100 nm, $\langle d \rangle$ = 0.1302327 nm, μ = 0.024200.
Rys. 4. Rentgenowskie profile dyfrakcyjne: doświadczalny (ciągły) i obliczony (przerywany) dla monokryształu ZnO implantowanego dawką 1 x 10^{14} cm^{-2}. Refleks 00·4, x_0 = 180 nm, σ = 100 nm, $\langle d \rangle$ = 0,1302327 nm, μ = 0,024200.

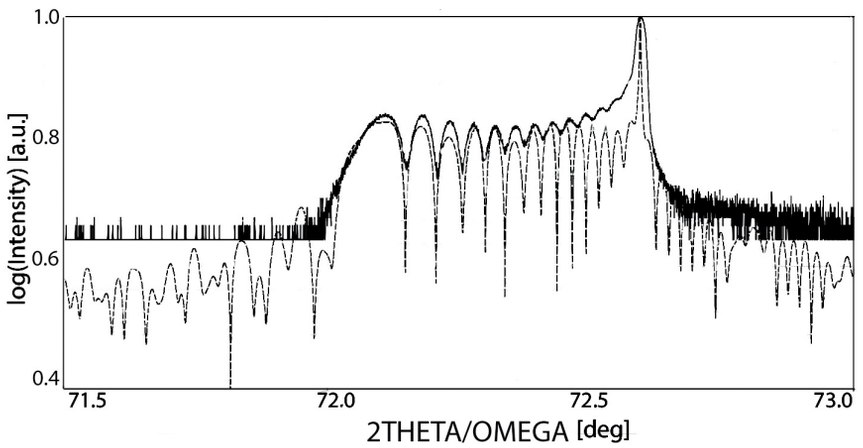

Fig. 5. X-ray diffraction profiles: experimental (solid) and calculated (dash) for the ZnO monocrystal implanted with the ion dose of 2 x 10^{15} cm^{-2}. Reflection 00·4, x_0 = 180 nm, σ = 140 nm, <*d*> = 0.1304943 nm, μ = 0.085291.
Rys. 5. Rentgenowskie profile dyfrakcyjne: doświadczalny (ciągły) i obliczony (przerywany) dla monokryształu ZnO implantowanego dawką 2 x 10^{15} cm^{-2}. Refleks 00·4, x_0 = 180 nm, σ = 140 nm, <*d*> = 0,1304943 nm, μ = 0,085291.

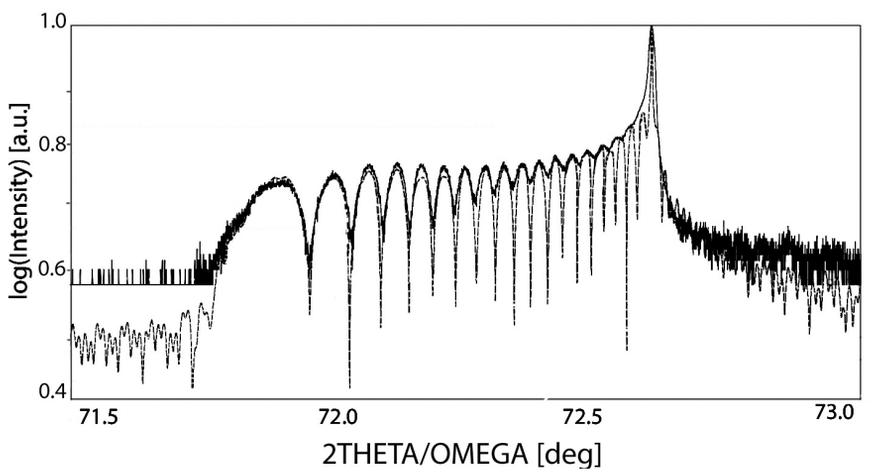

Fig. 6. X-ray diffraction profiles: experimental (solid) and calculated (dash) for the ZnO monocrystal implanted with the ion dose of 5 x 10^{15} cm^{-2}. Reflection 00·4, x_0=180 nm, σ = 120 nm, <*d*> = 0.1306206 nm, μ =0.139054.
Rys. 6. Rentgenowskie profile dyfrakcyjne: doświadczalny (ciągły) i obliczony (przerywany) dla monokryształu ZnO implantowanego dawką 5 x 10^{15} cm^{-2}. Refleks 00·4, x_0=180 nm, σ = 120 nm, <*d*> = 0,1306206 nm, μ = 0,139054.

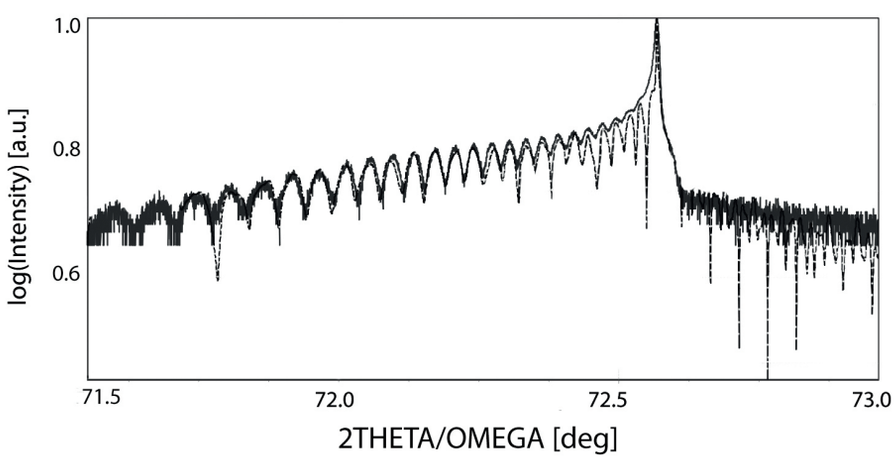

Fig. 7. X-ray diffraction profiles: experimental (solid) and calculated (dash) for the ZnO monocrystal implanted with the ion dose of 1 x 10^{16} cm^{-2}. Reflection 00·4, x_0=180 nm, σ = 130 nm, <*d*> = 0.1306401 nm, μ =0.143664.
Rys. 7. Rentgenowskie profile dyfrakcyjne: doświadczalny (ciągły) i obliczony (przerywany) dla monokryształu ZnO implantowanego dawką 1 x 10^{16} cm^{-2}. Refleks 00·4, x_0 = 180 nm, σ = 130 nm, <*d*> = 0,1306401 nm, μ = 0,143664.

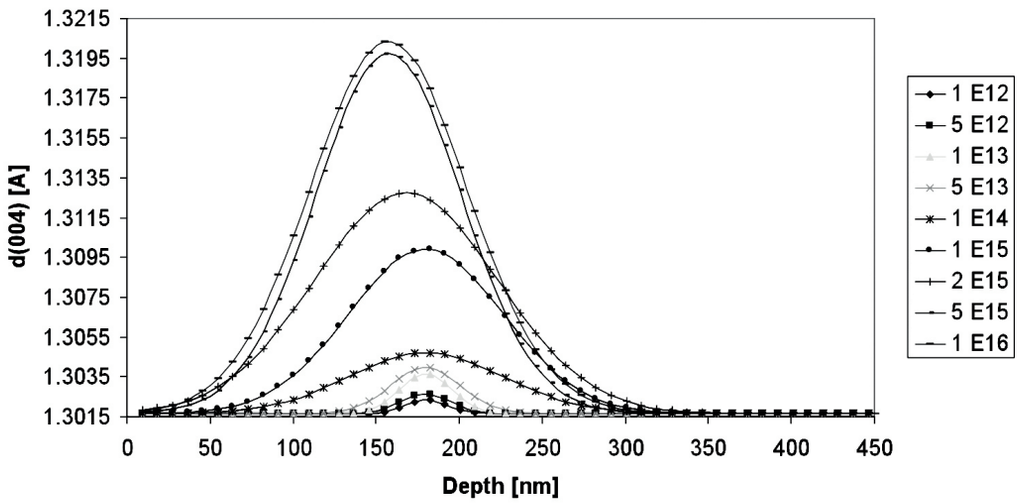

Fig. 8. Gaussian strain distributions induced in the Ar ion-implanted ZnO monocrystals.
Rys. 8. Gaussowski rozkład odkształceń wywołanych w monokrysztale ZnO na skutek implantacji jonów Ar.

Fig. 8 presents the Gaussian strain distributions for which the best fit between the experimental and calculated diffraction profiles was achieved. Each of the presented strain distribution was induced in the ZnO monocrystal through irradiation with different Ar-ion doses.

For doses equal to or higher than 2 x 10^{15}, in order to find a good fit between the calculated and measured X-ray diffraction profiles it was necessary to assume that the planar structure factor of (00·4) planes in the damaged region is reduced in comparison with that of the perfect crystal. It may be explained by the fact that as a result of irradiation, a fraction of the atoms is moved from their positions, out of the Bragg planes and cease to scatter coherently the X-ray photons. Computer calculation of the X-ray diffraction profile is carried out by employing the planar scattering factor, at the same time allowing its modification. In the case of the ZnO monocrystals, the formula describing the planar scattering factor of the (00·4) Bragg planes in the implanted volume of the crystal took the following form:

$$F_{00\cdot4}(x) = \xi(x)\,(f_{Zn}(x) + f_O(x)), \qquad (2)$$

where: f_{Zn} - the atomic factor of zinc, f_O - the atomic factor of oxygen, $(f_{Zn}(x) + f_O(x))$ - the planar scattering factor of the (00·4) Bragg planes in the non-implanted ZnO crystal and $F_{00\cdot4}$ is the planar scattering factor in the implanted ZnO region, as the largest shifts of Zn and O atoms from their Bragg position occupied in the perfect crystal could be expected only in the vicinity of the maximum of the standard strain distribution. The function $\xi(x)$ was defined as:

$$\xi(x) = 1 - \alpha \exp\left(\frac{-4 \ln 2(x - x'_0)^2}{\sigma_1^2}\right), \quad \alpha \in [0:1], \qquad (3)$$

where parameter α is determined during the search of the best fit between the theoretical and experimental profiles, σ_1 is the full width at half maximum and x'_0 is the position of the maximum of the Gaussian function. In this work we assumed an equal reduction of the atomic scattering factors of both oxygen and zinc.

Fig. 9 presents the $\xi(x)$ functions for 2 x 10^{15}, 5 x 10^{15} and 1 x 10^{16} cm^{-2} ion doses.

A convenient measure of the crystalline order characterization of the implanted ZnO monocrystal is the parameter characterizing a degree of amorphization η, ranging from $\eta = 0$ for the implanted volume in which all atoms are in their correct Bragg position, to $\eta = 1$ for the amorphic material with all atoms moved out of their Bragg positions, and is defined as follows:

$$\eta = \frac{1}{D}\int_0^D (1 - \xi(x))\,dx = \frac{\alpha}{D}\int_0^D \exp\left(\frac{-4 \ln 2(x - x'_0)^2}{\sigma_1^2}\right) dx, \qquad (4)$$

where: η is the degree of amorphization, and D denotes the total width of the implanted region.

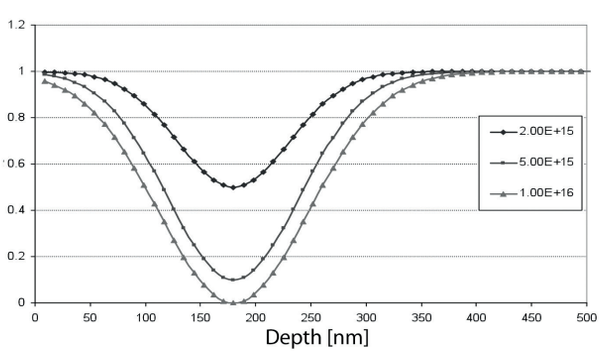

Fig. 9. $\xi(x)$ functions for 2 x 10^{15} cm^{-2}, 5 x 10^{15} cm^{-2} and 1 x 10^{16} cm^{-2} ion doses, obtained to ensure the best fit between the theoretical and experimental diffraction profiles.
Rys. 9. Funkcja $\xi(x)$ dla dawek 2 x 10^{15} cm^{-2}, 5 x 10^{15} cm^{-2} i 1 x 10^{16} cm^{-2} otrzymana dla najlepszego dopasowania rentgenowskich profili dyfrakcyjnych doświadczalnych i obliczonych.

Tab. 1. Parameters of strain distribution and ξ(*x*) function for the ZnO monocrystals implanted to different doses of Ar ions.
Tab. 1. Parametry rozkładu odkształceń oraz funkcja ξ(x) dla monokryształu ZnO implantowanego kolejnymi dawkami jonów Ar.

Ion dose [cm^{-2}]	μ	Average misfit $\Delta a/a$ [ppm]	Average interplanar spacing [nm]	σ [nm]	σ_1 [nm]	x'_0 [nm]	x_0 [nm]	α	Degree of amorfization η
5 x 10^{11}	0.001906	12	0.1301666	30	-	-	180	0	0
1 x 10^{12}	0.002151	29	0.1301688	30	-	-	180	0	0
5 x 10^{12}	0.003457	64	0.1301733	35	-	-	180	0	0
1 x 10^{13}	0.015365	93	0.1301771	37	-	-	180	0	0
5 x 10^{13}	0.017669	190	0.1301897	50	-	-	180	0	0
1 x 10^{14}	0.024200	520	0.1302327	100	-	-	180	0	0
1 x 10^{15}	0.059923	2100	0.1304383	160	-	-	180	0	0
2 x 10^{15}	0.085291	2530	0.1304943	140	120	180	180	0.5	0.13
5 x 10^{15}	0.139054	3500	0.1306206	120	140	180	180	0.9	0.24
1 x 10^{16}	0.143664	3650	0.1306401	130	160	180	180	1.0	0.35

The $\alpha = 0.5$ and $x_0 = 180$ nm values mean that in the atomic plane located at the depth of 180 nm at least 50% of atoms were displaced from their regular Bragg lattices sites. For $\alpha = 1$, all atoms from this plane were displaced. In tab. 1, the average strain values calculated for ion doses of 2 x 10^{15}, 5 x 10^{15} cm^{-2} and 1 x 10^{16} cm^{-2} were presented, assuming that amorphization did not occur. Then, these values were overestimated. The same applies to the interplanar spacings.

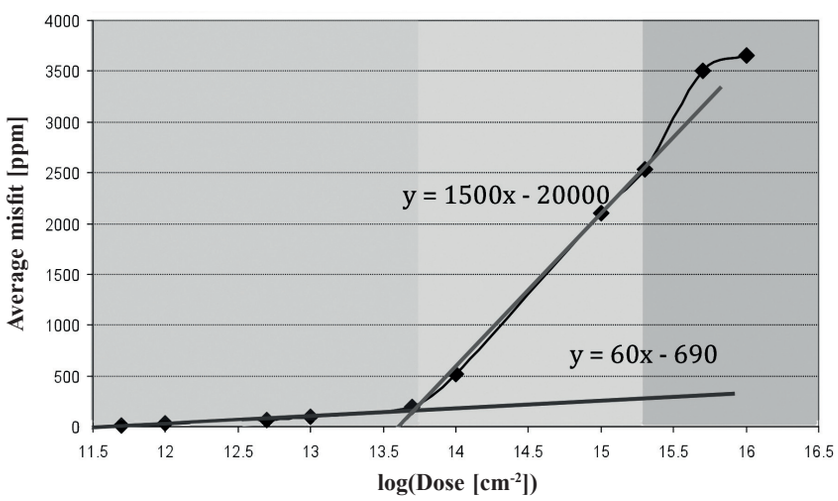

Fig. 10. The average misfit between the implanted layer and the remainder of the ZnO monocrystal.
Rys. 10. Srednie niedopasownie sieciowe pomiędzy implantowaną i pozostałą objętością monokryształu ZnO.

In Tab. 1 the main structural parameters are listed, thus yielding the best fit between the experimental and calculated X-ray diffraction profiles.

The average misfit between the implanted layer and the remainder of the ZnO monocrystal is shown in Fig. 10.

Three regions can be distinguished. The first region ranges from 5 x 10^{11} cm^{-2} to 5 x 10^{13} cm^{-2}, the second one from 5 x 10^{13} cm^{-2} to 1 x 10^{15} cm^{-2}, and finally the third one is above 1 x 10^{15} cm^{-2}. In the first region, the dependence between the ion doses and the average misfit $\Delta a/a$ in the whole implanted region can be presented in the following form:

$$\frac{\Delta a}{a} = 60 \log(I) - 690$$

In the second region, the same relation is shown as:

$$\frac{\Delta a}{a} = 1500 \log(I) - 20000$$

There is no linear dependence in the third region.

3. Discussion

Strain development is a vital clue to understanding damage accumulation and its transformation in ZnO. Every displaced atom produces quasi-hydrostatic pressure in the lattice cell. Since the bombarded lattice is constrained by the underlying, undamaged crystal to expand only in a direction perpendicular to the surface, the implanted layer is in the lateral compression and gives the strain distribution. Consequently, the tetragonalization of the lattice cell can be measured by HRXRD. Our study shows the growth of tetragonalization of the ZnO unit cell versus the ion implantation dose. This effect may be created due to the agglomeration of vacancies and interstitial atoms. These processes seem to last until a particular critical stress value is reached before eventually transformation to Stage II takes place. This is typical for plastic deformation. A similar case of transformation was described for GaN, in which the tensile stress was produced by extended defects, also causing the lattice spacing increase (compatible with the Hook's law). Once the yield point had been reached, transformation to Stage II was driven by plastic deformation and the release of stress could be observed [14 - 17]. The resemblance between HRXRD profiles for both materials implies that most likely similar processes occur in ZnO.

4. Conclusions

Damage accumulation in compound single crystals such as some oxides ($SrTiO_3$, ZrO_2, $MgAl_2O_4$) or GaN, appears to be a complex, multi-step process [18 - 19]. The key driving force is the elastic strain in the damaged region, which develops in the bombarded areas. It is induced by simple defect agglomeration, resulting in the formation of stacking faults, faulted loops or dislocations. Based on the results described in this paper it can be concluded that the defect behavior in ZnO follows a similar pattern.

Moreover, it has been shown clearly that the damage buildup in compound crystals should be studied using HRXRD analysis of the shift of atoms from their position on the Bragg planes.

References

[1] Özgür Ü., Alivov Y. I., Liu C., Teke A., Reshchikov M. A., Doğan S., Avrutin V., Cho S. J., Morkoç H.: A comprehensive review of ZnO materials and devices, *J. Appl. Phys*., 2005, 98, 041301

[2] Kucheyev S. O., Williams J. S., Jagadish C., Zou J., Evans C., Nelson A. J., Hamza A. V.: Ion-beam-produced structural defects in ZnO, *Phys. Rev. B,* 2003, 67, 094115

[3] Wendler E., Bilani O., Gärtner K., Wesch W., Hayes M., Auret F. D., Lorenz K., Alves E.: Radiation damage in ZnO ion implanted at 15 K, *Nucl. Instr. Meth.,* 2009, B267, 2708 – 2711

[4] Azarov A. Y., Hallen A., Du X. L., Rauwel P., Kuznetsov A.Y., Svenson B. G.: Effect of implanted species on thermal evolution of ion-induced defects in ZnO, *J. Appl. Phys*., 2014, 115, 073512.

[5] Turos A.: On the mechanism of damage buildup in gallium oxide, *Radiation Effects & Defects in Solids*, 2013, 168, 431

[6] Wojcik M., Gaca J., Wierzbicka E., Turos A., Strupiński W., Caban P., Sathish N., Pągowska K.: Lattice strain study In implanted GaN epitaxial layer deposited by means of MOCVD technique on [001] oriented sapphire substrate, *Electronic Materials*, 2011, 39, 4, 22 – 31

[7] Jagielski J., Jozwik P., Jozwik-Biala I., Kovarik L., Arey B., Gaca J., Jiang W.: RBS/C, HRTEM and HRXRD study of damage accumulation in irradiated $SrTiO_3$, *Radiation Effects & Defects in Solids*, 2013, 6, 168, 442 – 449

[8] Durbin S. M., Follis G. C.: Darwin theory of heterostructure diffraction. *Phys. Rev. B,* 1995, 51, 10127 – 10133

[9] James R. W.: The optical principles of the diffraction of X-rays, Vol. 2, G. Bell And Sons Limited, 1962, London

[10] Gaca J., Wójcik M., Bugajski M., Kosiel K.: The determination of the chemical composition profile of the GaAs/AlGaAs heterostructures designed for quantum cascade lasers by means of synchrotron radiation, *Radiation Physics and Chemistry*, 2011, 80, 1112 – 1118

[11] Dygo A., Turos A.: Surface studies of $A^{III}B^{V}$ compound semiconductors by ion channeling, *Phys. Rev. B,* 1989, 40, 7704

[12] Nowicki L., Turos A., Ratajczak R., Stonert A., Garrido F.: Modern analysis of ion channeling data by Monte Carlo simulations, *Nucl. Instr. and Meth. B*, 2005, 240, 277

[13] Turos A., Jozwik P., Nowicki L., Sathish N.: Ion channeling study of defects in compound crystals using Monte Carlo simulations, *Nucl. Instr. and Meth. B*, 2014, 332, 50

[14] Ratajczak R., Turos A., Stonert A., Nowicki L., Strupinski W.: Defect transformations in ion bombarded InGaAsP, *Acta Phys. Polonica A*, 2011, 120 (1), 136

[15] Pagowska K., Ratajczak R., Stonert A., Nowicki L., Turos A.: Compositional dependence of damage

buildup in Ar-ion bombarded AlGaN, *Vacuum*, 2009, 83, S145 – S147

[16] Guziewicz E., Kowalik A., Godlewski M., Kopalko K., Osinniy V., Wójcik A., Yatsunenko S., Łusakowska E., Paszkowicz W., Guziewicz M. et al.: Extremely low temperature growth of ZnO by atomic layer deposition, *J. Appl. Phys*., 2008, 103, 3, 033515

[17] Turos A., Gaca J., Wojcik M., Nowicki L., Ratajczak R., Groetzschel R., Eichhorn F., Schell N.: Virtues and pitfalls in structural analysis of compound semiconductors by the complementary use of RBS/channeling and high resolution X-ray diffraction, *Nuclear Instruments and Methods in Physics Research B,* 2004, 219 – 220, 618 – 625

[18] Devaraju G., Dhamodaran S., Pathak A. P., Saravanan S. G., Gaca J., Wojcik M., Turos A., Khan S. A., Avasthi D. K., Arora B. M.: Ion beam modification of strained InGaAs/InP characterized by HRXRD, PL and AFM, *Nuclear Instruments and Methods in Physics Research B,* 2008, 266, 3552 – 355

[19] Eichhorn F., Gaca J., Heera V., Schell N., Turos A., Weishart H., Wojcik M.: Structural studies on ion-implanted semiconductors using X-ray synchrotron radiation:Strain evolution and growth of nanocrystals, *Vacuum,* 2005, 78, 303 – 309